

Study on aerodynamic coefficients and responses of the integrated catwalk of Halogaland Bridge

Jia-wei Wan^{1a}, Qi Wang^{*2}, Hai-li Liao^{2b} and Ming-shui Li^{2c}

¹Department of Bridge Engineering, Southwest Jiaotong Univ., Chengdu, Sichuan, 610031 China

²Department of Bridge Engineering and Research Center for Wind Engineering, Southwest Jiaotong Univ., Chengdu, Sichuan, 610031 China

(Received December 28, 2016, Revised August 13, 2017, Accepted August 17, 2017)

Abstract. Wind tunnel tests and numerical aerodynamic analyses were conducted for an integrated catwalk structure under strong winds. From the wind tunnel tests, it is found that the aerodynamic coefficients were different from those of the typical type. The drag coefficient was larger than typical and was sensitive to number of vertical meshes installed rather than the solidity ratio. Comparing with typical catwalk, the integrated one showed larger deformation under strong wind, and the large torsional deformation are mainly caused by drag force. It did not show aerodynamic divergence even the torsional deformation reaching 20°. The reason could be that the stiffness is smaller and thus the catwalk is able to deform to the shape compactable with higher loading. Considering safety for construction, storm rope system is introduced to the catwalk to reduce the deformation to acceptable level.

Keywords: suspension bridge; integrated catwalk; wind tunnel test; static response; nonlinear analysis

1. Introduction

Catwalks, naming for temporary suspended walkways, are installed to assist the erection of main cables for suspension bridges. For most suspension bridge construction in the past, usually catwalks are installed separately on each main cable, since there is large spacing between the main cables. The typical catwalk structures, paralleling in pair, are shown in Fig. 1 (Kwon *et al.* 2012).

Catwalk structure consists of a few ropes, cross beams, wooden steps, and porous wire meshes at the bottom and both sides. The ropes support the weight of workers and equipment during cable erection, and also the weight of a main cable wire. There are portal frames installed on each catwalk structure at certain spacing and the pair of catwalk structures are linked with connecting bridges at regular intervals.

In the past, wind-induced effects on typical catwalk structures have been well studied and have obtained extensive knowledge about the aerodynamic behaviors during its construction. To make this paper simple and short, readers that are interested in previous research and research objectives

*Corresponding author, Assistant Professor, E-mail: wangchee_wind@swjtu.edu.cn

^a Ph. D. student, E-mail: jiawei.wan@outlook.com

^b Professor and Director, E-mail: hlliao@swjtu.edu.cn

^c Professor and Vice Director, E-mail: lms_rwe@126.com

on typical catwalks can refer to the summary presented in “Dynamic wind actions on catwalk structures” (Kwon *et al.* 2012).

The following study object, the catwalk structure to be built for Halogaland Bridge in Norway, is quite different from the typical. It is not in pair but an integrated one, since the main cables are very close to each other (see Fig. 2) during cable installation stage. The integrated catwalk will be divided into two separate ones once commencing bridge deck erection. For easy understanding, plan view of main cable at final stage is shown in Fig. 3.

Apparently, the integrated catwalk is more easily to have aerodynamic divergences since its stiffness is smaller. Moreover, aerodynamic study regarding this rare type of catwalk could hardly be found from current available research. Consequently, exploratory studies, presented in the following sections, have been done to this integrated type by both wind tunnel test and finite element simulation method.

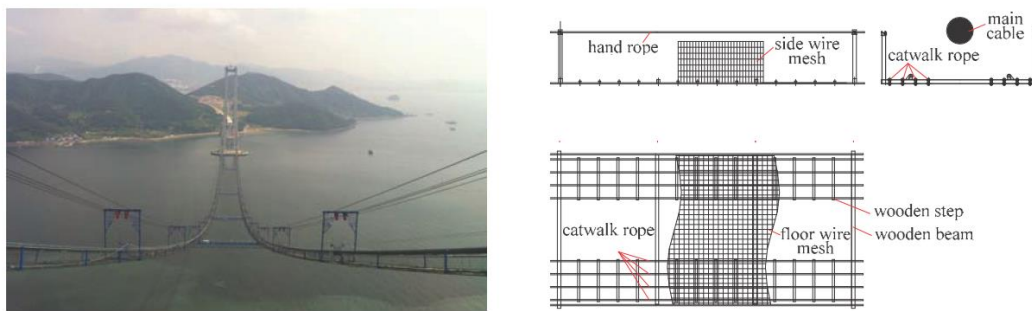


Fig. 1 Typical catwalk structures

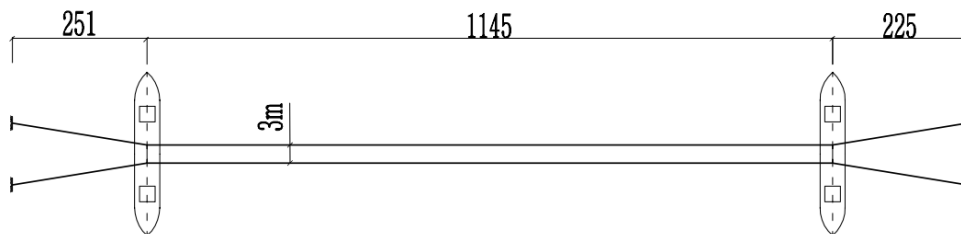


Fig. 2 Plan view of main cables during cable installation stage

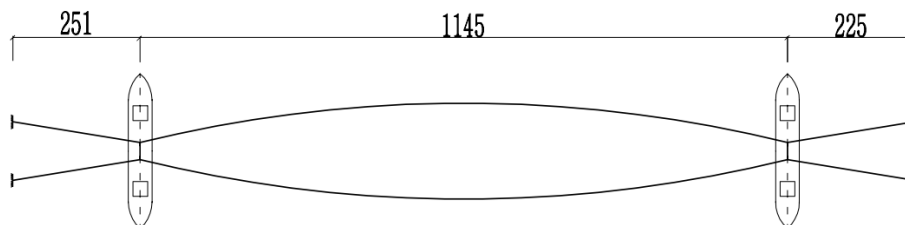


Fig. 3 Plan view of main cables at final stage (indicative only)

2. Wind tunnel tests

2.1 Catwalk system

The target model, shown in Fig. 4, is proposed by Sichuan Road and Bridge Group Company (SRBG). Section model is built according to the proposed design. Wind tunnel tests are carried out to investigate its aerodynamic behaviors and found the design to be further optimized. The finalized catwalk design was submitted to SRBG for construction use.

As shown in Fig. 4, the width and height of the catwalk are 7.0 m and 1.5 m, respectively. Two duplicate segments, each part 3.5 m wide, are assembled together along one edge to form the integrated one. Such design, with two wire meshes at the middle, has considered that the two duplicate parts will be finally separated during bridge deck erection. Each duplicate segment consists of six floor supporting ropes, two hand ropes on each side, steel tube cross beam, and a set of safety components including wire mesh, wooden steps and hand rope posts. The solidity ratios of the side/middle and floor were 17% and 21%, respectively. Tramway portal frame, shown in Fig. 5, is fixed on the catwalk at a spacing of 50 m to enhance the stiffness.

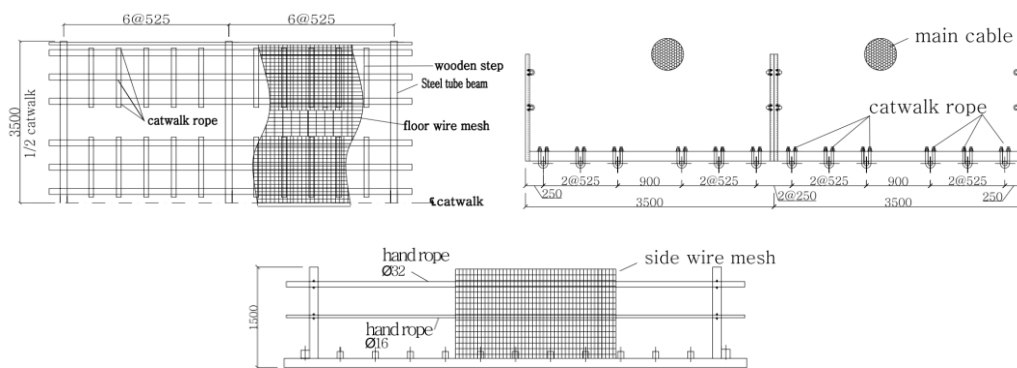
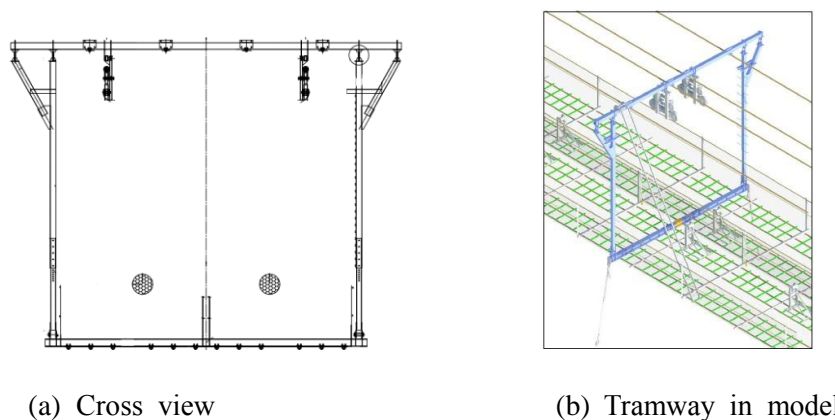


Fig. 4 Integrated catwalk system



(a) Cross view

(b) Tramway in model

Fig. 5 Tramway portal frame

2.2 Experimental setup

A rigid model with scale of 1/10 scale (0.7 m wide \times 0.15 m high \times 2.1 m long) was fabricated and tested in wind tunnel to obtain the aerodynamic coefficients of the catwalk. To make the model rigid enough, the floor supporting ropes and steel tube cross beams are made of steel and welded together. The wire mesh solidity ratio, which determines the wind forces acting on the catwalk, should be exactly the same as that of actual structure.

Similar to research on typical catwalks, solidity ratio effects on aerodynamic coefficients are investigated by changing the wire mesh arrangement. Three test models, with same floor solidity ratio, are shown in Fig. 6. It is important to fix the floor ratio because the catwalk will be separated at bridge deck erection stage. During construction, once the two duplicate parts are separated, additional wire mesh can be installed on its open side. For the test models, Model II is the modified version of Model I by removing its middle mesh and Model III are modified version of Model II by changing the side meshes.

Wind tunnel tests are carried out at XNJD-1 wind tunnel Section II in Southwest Jiaotong University. The tunnel test section size is 2.4 m wide \times 2.1 m high \times 10 m long and the turbulent intensities are less than 0.5%. Photo of the section model setting up is shown in Fig. 7.

Aerodynamic forces acting on the model were measured using a pair of force balances which can provide reading for three forces and the associated three moments. The mean wind speed was measured by a pitot tube and a pressure transducer. Attack angles varied from -10° to $+10^\circ$ at 1 degree interval. The tests were conducted under two sets of wind speed, 15 m/s and 18 m/s respectively.

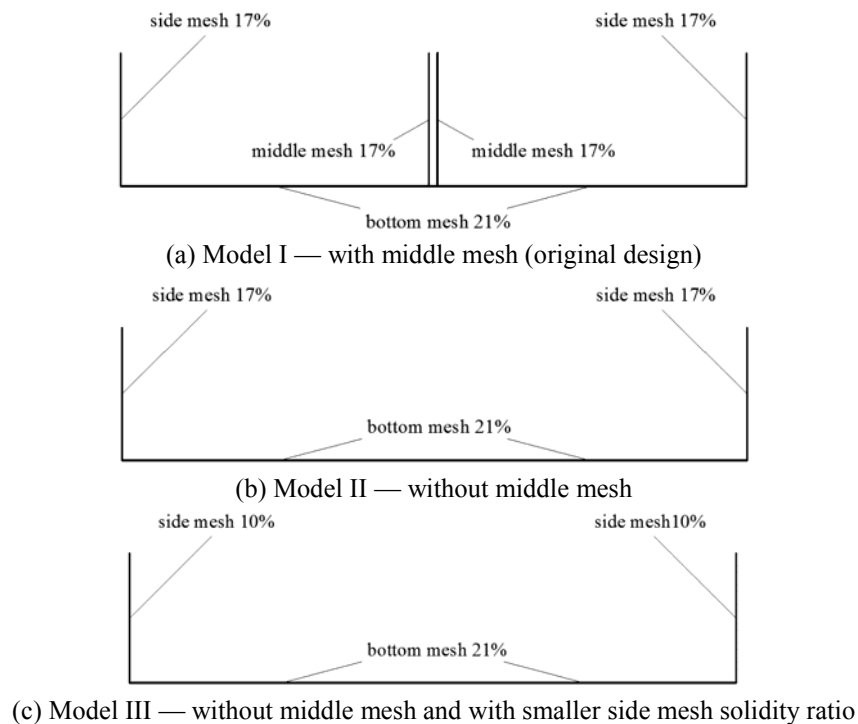


Fig. 6 Wire mesh arrangement for test models



Fig. 7 Section model in wind tunnel

Based on previous study, Reynolds number effect on aerodynamic coefficients can be neglected. So the test was set up only based on geometric and solidity similarity principles. Meanwhile, the correction for the blockage effect was not done since the blockage ratio of the model was less than 2%.

The forces and moments were transformed into non-dimensional aerodynamic coefficients using the following equations

$$F_x(\alpha) = \frac{1}{2} \rho U^2 H L C_D(\alpha) \quad (1)$$

$$F_y(\alpha) = \frac{1}{2} \rho U^2 H L C_L(\alpha) \quad (2)$$

$$M_x(\alpha) = \frac{1}{2} \rho U^2 H L C_M(\alpha) \quad (3)$$

Where, α is the attack angle; ρ is the air density, which is 1.225 kg/m³, U is wind speed; H , B , and L are the height, width and length of the section model respectively. C_D , C_L and C_M are drag force, lift force, and pitching moment respectively.

2.3 Test results

Aerodynamic coefficients from tests are shown in Fig. 8. The drag coefficients of this integrated catwalk are much larger, almost twice comparing with those under typical type from reference (Ito *et al.* 1976).

For easy calling, the middle mesh and side mesh can be considered as vertical mesh. It can see that the solidity ratio of vertical mesh strongly affects the drag coefficient. The higher the vertical solidity ratio is, the larger the drag coefficient. The lift and pitching moment coefficients are more related to number of vertical meshes installed rather than the solidity ratio of the vertical member, as they only show noticeable variance between cases with/without middle mesh but almost no difference for cases without middle mesh even the side mesh solidity ratio varied. Apparently, Model I with middle mesh also produced largest lift and pitching moment coefficients amongst the three

test models. As such, it is advised to remove the middle mesh to reduce both the aerodynamic coefficients and the possibility of aerodynamic divergences. The solidity ratio of side mesh should be as small as possible.

2.4 Design formulas for aerodynamic coefficients

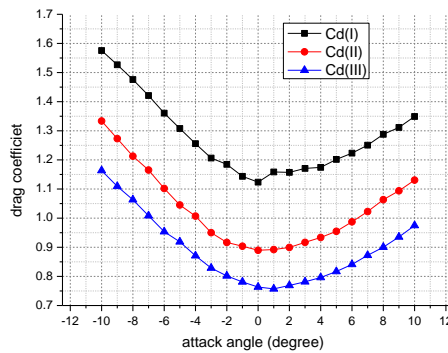
Based on test results from Model III, with 21% floor solidity ratio and 10% side solidity ratio respectively, fitting equations for aerodynamic coefficients are generated as follows

$$C_D(\alpha) = 0.7792 - 0.0096\alpha + 0.00305\alpha^2 \tag{4a}$$

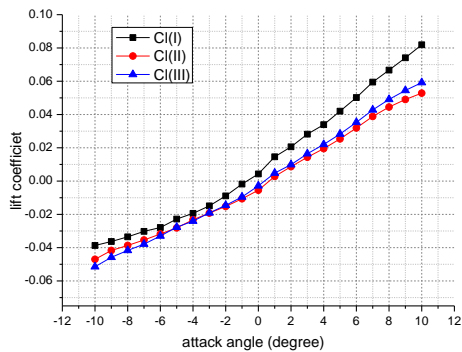
$$C_L(\alpha) = 0.00564 - 0.002\alpha + 0.00007443\alpha^2 \tag{4b}$$

$$C_M(\alpha) = 0.00512 - 0.0003162\alpha - 0.00004312\alpha^2 \tag{4c}$$

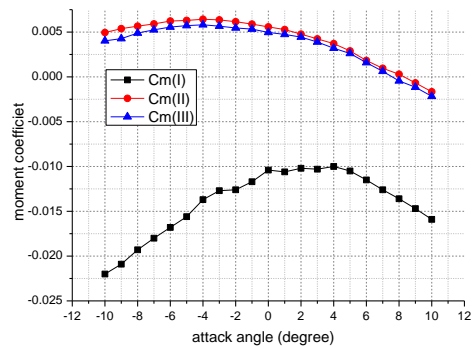
where α is attack angle in degree.



(a) Drag coefficient

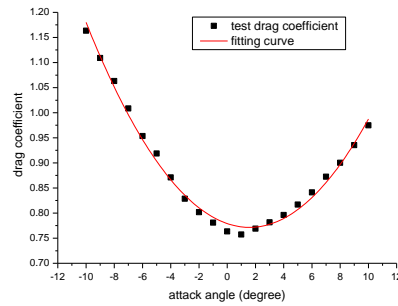


(b) Lift coefficient

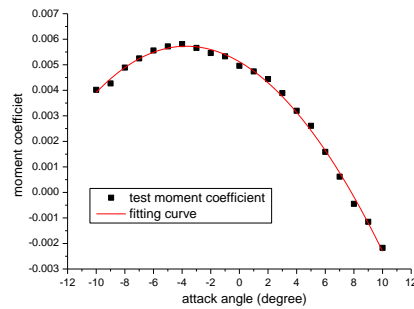


(c) pitching moment coefficient

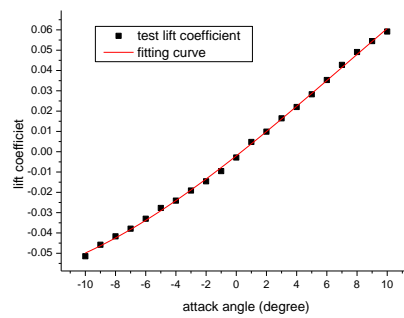
Fig. 8 Time averaged aerodynamic coefficients



(a) The fitting curve of drag coefficient



(b) The fitting curve of moment coefficient



(c) The fitting curve of lift coefficient

Fig. 9 Fitting curve of the coefficients

Fig. 9 shows the aerodynamic coefficients from test and the above design equations. It indicates that the lift and pitching moment coefficients can accurately match the test results by using fitting equations. For drag coefficient, the accuracy of fitting equations between -2° to $+2^\circ$ attack angle is relatively lower and accuracy for attack angle beyond this range can be considered very high.

3. Aerostatic response analysis

3.1 Theory of static deformation of integrated catwalk

In this paper, the following theory for aerodynamic response of the integrated catwalk was proposed to identify the cause of unique behaviour. Two simplified models (Fig. 10), referring to free pendulum motion, one have three ropes (Model A) only and the other have three ropes fixed by a cross beam (Model B), were developed to demonstrate the deformation characteristics of the integrated catwalk.

Model A, shown in Fig. 10(a), is simulation for free pendulum motion. If the ropes subjected to a lateral uniform force, the three ropes would rotate independently and have the same deformation. The same lateral and vertical displacements of the ropes can be easily obtained based on the rotation angle ϕ . Under static wind load, it can see the horizontal drag force not only directly cause lateral displacement but will also induce vertical and torsional displacement.

Model B, shown in Fig. 10(b), the three ropes will deform as a whole element due to connected by the cross beam. The deformation of the three ropes is no longer the same. The windward rope had longer lateral displacement but shorter vertical displacement, and the leeward one is reversal.

Some brief formulas were proposed below to obtain the lateral and vertical displacement of cross beams or ropes, but the torsion of the cross beam is different due to distinct varying axial stress and stiffness along the rope. The rotation at pylon top is zero since its end is fixed. On this condition, the torsion of cross beam can be calculated according to the compatible status between deflection and stress.

The equations for the three lateral displacements, middle rope L , windward rope L_1 and leeward rope L_2 are as follows

$$L = \sin\phi \tag{5a}$$

$$L_1 = R_m \sin\phi - K \cos\phi' \tag{5b}$$

$$L_2 = R_m \sin\phi + K \cos\phi' \tag{5c}$$

where, R_m is the sag of suspension rope for span centre, for other location it is the local sag from the pylon top; K is the rope spacing, and ϕ is the torsion of the whole section induced by drag force, and ϕ' is the torsion of cross beam. For rope at the sag, the slope effect on rope stress can be ignored, so the torsion of the cross beam can be assumed equal to rotating angle ϕ' .

The vertical displacements for middle rope D , windward rope D_1 and leeward rope D_2 can be expressed as follows.

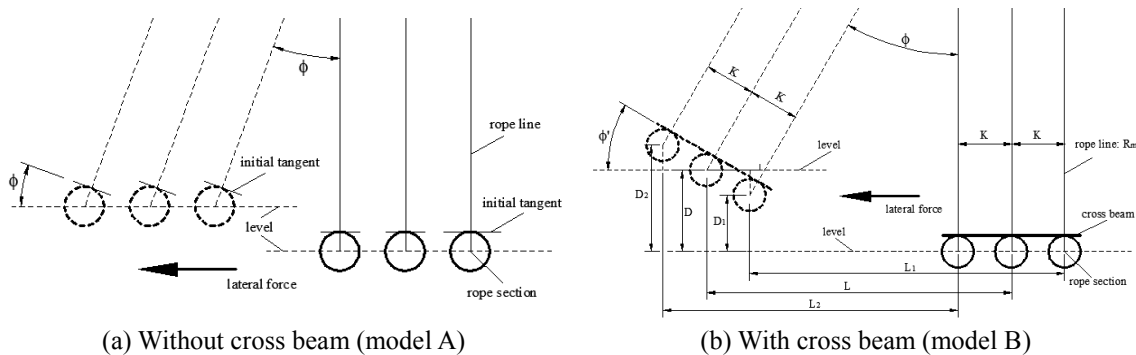


Fig. 10 Simplified model of integrated catwalk system

$$D = R_m (1 - \cos\phi') \quad (6a)$$

$$D_1 = R_m (1 - \cos\phi') - K \sin\phi' \quad (6b)$$

$$D_2 = R_m (1 - \cos\phi') + K \sin\phi' \quad (6c)$$

The final torsion of catwalk or cross beam, θ , could be expressed, the rotating angle only induced by drag force, plus angle ϕ , which induced by pitching moment, is as follows

$$\theta = \phi' + \phi \quad (7)$$

The final transitional motion should be updated based on the local angle θ , and the vertical displacement also needs to add the vertical displacement h caused by lift force.

The Eq. (7) implied that the torsional and vertical deformation are mainly induced by the large lateral displacement rather than the tiny angle ϕ that induced by the small pitching moment, and this was very different from bridge deck torsional behaviour which is mainly produced by pitching moment.

Equations 6(a)-6(c) indicate that the torsional displacements were strongly coupled with the lateral ones, which were mainly induced by drag force. For integrated catwalk, the lateral displacement can be very large since its lateral stiffness is very small. Although the portal frame can strengthen the local stiffness of passway evidently, it only acts as local rigid constrain for supporting ropes, but not rigid enough as connecting bridge that can improve the stiffness significantly.

For the physical catwalk structure, when there is the wind flow, the lateral displacement is so evident that can induce dramatic torsion, and the increased torsion could cause additional wind load, especially for drag force. Therefore the deformation of the structure should be modified with the additional aerodynamic wind load consequently. The static balance will appear until the resistance of the structure and wind load is equal to each other. Actually, the wind velocity is not the same along the height profile, and there is also dramatic stiffness variance along the structure, both of which will induce deformation variance, so the final deformation will be in shape of non-smooth and non-homogeneous curves, especially in torsion. The characteristics of aerodynamic response of integrated catwalk will be discussed concretely in the following sections with numerical method.

3.2 Finite element modelling

Finite element model was developed in ANSYS shown in Fig. 11. The model mainly included the major structural elements, such as the floor supporting ropes, steel tube cross beams and the portal frame system etc. Supporting ropes of the catwalk (walkway and portal frame) were assigned as cable element, for which the geometric stiffness depends on the internal axial force. Other elements were modelled using beam element. Non-structural elements including the manrope, handrails, and protective mesh were not physically incorporated in the model. However, these non-structural elements were considered as masses in the modelling input for accurate dynamic analysis.

3.3 Nonlinear analysis method

Further to 3.1, the aerodynamic response of the catwalk can be calculated by solving the following nonlinear iteration equation (Thai and Kim 2011), where the geometric nonlinearity and the nonlinear dependence of wind load on attack angle are incorporated.

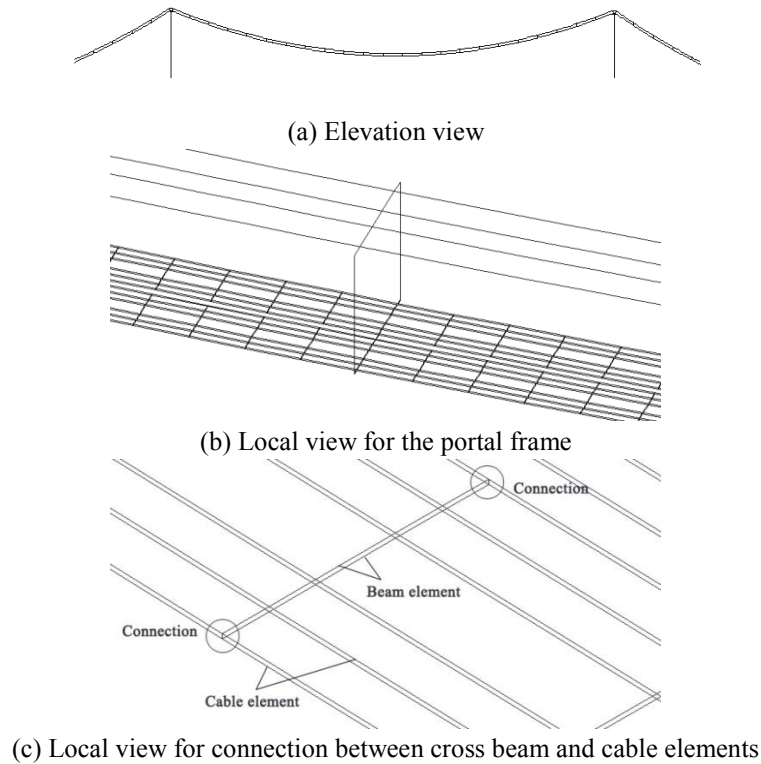


Fig. 11 Finite element model of the catwalk

$$[K_e(\{X_n\}) + K_g^{G+W}(\{X_n\})]\{X_{n+1}\} = \{F(\alpha_n)\} \quad (8)$$

Where, $[K]_e$ and $[K]_g$ represent the elastic stiffness and geometric stiffness of structure matrix respectively, and the latter acts as the major part in a long span suspension cable structure; $\{X\}$ is the displacement vector; α_n is effective attack angle; $\{F\}$ represents the external wind force vector including aerodynamic effects; the subscript n represents the n^{th} solving target position, and $n+1$ means the adjacent position; and superscript G and W represent geometric stiffness due to gravity and wind-induced load.

The convergence for a given wind velocity can be obtained when the Euclidean norm of the aerodynamic coefficients C_k is less than the prescribed tolerance, which is

$$\frac{\sum_N [C_k(\alpha_{n+1}) - C_k(\alpha_n)]^2}{\sum_N [C_k(\alpha_n)]^2} \leq \varepsilon \quad (9)$$

where ε is the prescribed tolerance and N is the number of nodes subjected to the wind loads. Since wind load for long span bridge is displacement-dependent, it is necessary to extract the catwalk's

torsional deformation at every point and accordingly update the attack angle at every position. With the varying aerodynamic load at every position, it is able to develop the deformation shape along the catwalk. Same as aerodynamic analysis for girder in long span bridge, the incremental method, combined with internal iteration method and external iteration method was adopted to obtain the aerodynamic response (Cheng *et al.* 2002). The analysis takes account of both large displacement effect and nonlinearity of aerodynamic forces. At given wind speed, the internal iteration method was applied to update the stiffness while the external iteration method was adopted to identify the deformation in equilibrium. The detailed analysing procedure can be found in the references (Shinichi 1997).

3.4 Results of aerostatic response analysis

3.4.1 Drag force on deformation of integrated catwalk

In section 3.1, it is pointed that the drag force is the main cause of deformation for integrated catwalk and also contributes the majority of torsional deformation. This has been verified by the analysing results shown in Fig.12.

3.4.2 Study for aerostatic response at +3° attack angle

The aerodynamic response analysis were carried out under three initial attack angles, i.e., 0°, -3° and +3°, with input of exponential wind profile above 10 m ground level and wind speeds ranging from 10 m/s to 25 m/s.

A full study on the aerodynamic response of the integrated catwalk is carried out based on attack angle of +3°. The results are shown in Fig. 13-15.

As presumed, the catwalk displacements increase as wind speed going up. Both maximum lateral and vertical displacements occur at the center of main span, and the displacements do not increase in proportion to wind pressure due to large torsional deformation causing nonlinear wind pressure.

For the integrated catwalk, the torsional stiffness is only provided by the portal frames and the floor supporting ropes. Therefore, the torsional deformations are smaller where portal frames exist, while the maximum torsional deformation occurs at the center in between of two adjacent portal frames. Although torsional deformation distribution along spanwise is similar to that of typical type (Li *et al.* 2014), unlike the typical catwalk having the connecting bridge acting as the torsional restraint, the torsional stiffness of integrated type reduces sharply due to significantly larger torsional deformation.

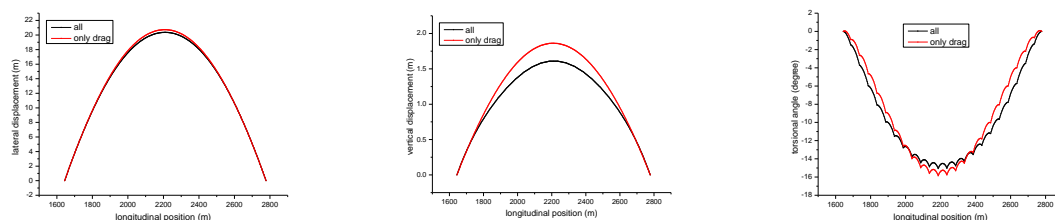
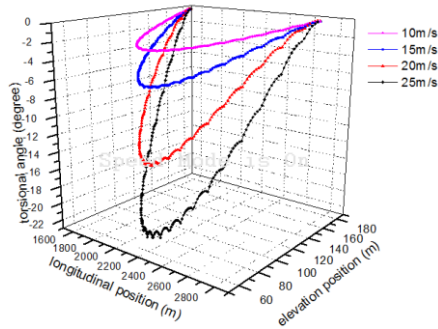
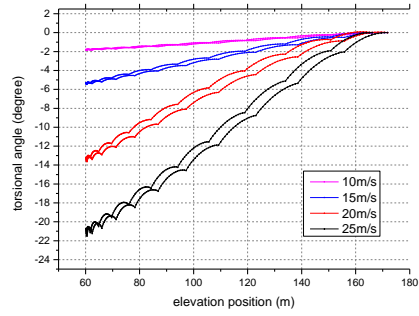


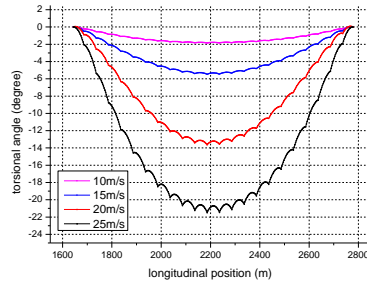
Fig. 12 Deformation due to drag force



(a) 3D view

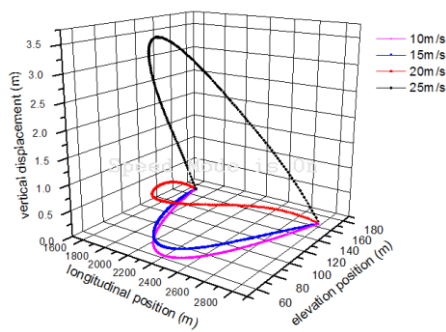


(b) Displacement along elevation

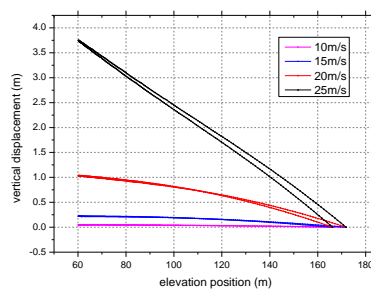


(c) Displacement along longitudinal axis

Fig. 13 Torsional displacement of catwalk

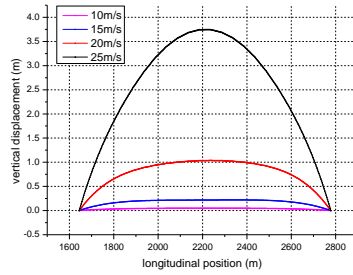


(a) 3D view



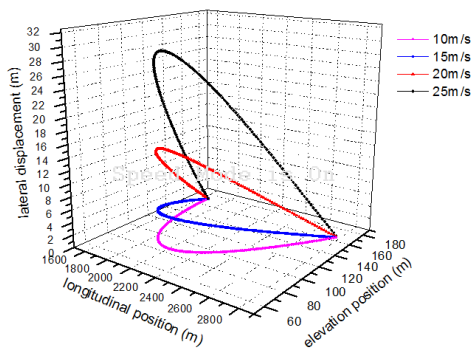
(b) Displacement along elevation

Continued-

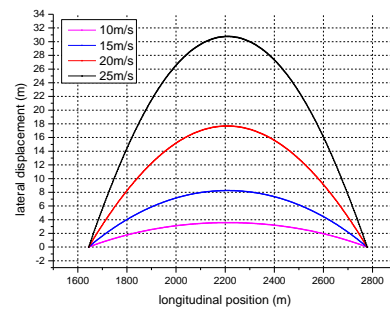


(c) Displacement along longitudinal axis

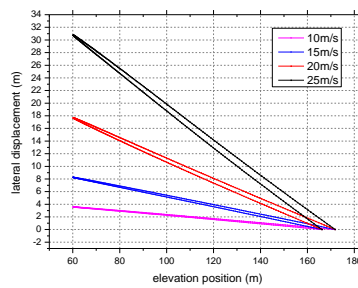
Fig. 14 Vertical displacement of catwalk



(a) 3D view



(b) Displacement along elevation



(c) Displacement along longitudinal axis

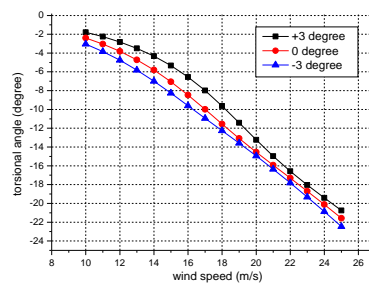
Fig. 15 Lateral displacement of catwalk

From common sense, the above summarize should also be applicable to the catwalk deformation under other attack angles. Response results under other two attack angles will not be presented as unnecessary.

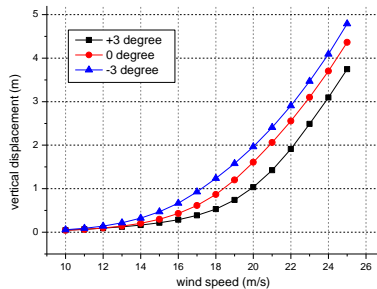
3.4.3 Maximum deformation under different attack angles

As pointed, the maximum deformation of the integrated catwalk located at span center. As known, it is critical to control the maximum deformation for catwalk design, so deformation study is focused on the maximum deformation only.

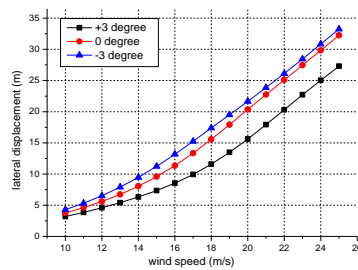
Fig. 16 presents the maximum deformation of the catwalk under different attack angles. All deformations, including lateral, vertical and torsional, under positive attack angle are smaller than those under zero and negative attack angles. The torsional deformation is always negative as the lifting force due to positive attack angle can counteract the cable stiffness under gravity.



(a) torsional



(b) vertical



(c) lateral

Fig. 16 Displacement of catwalk at different initial wind angle of attack

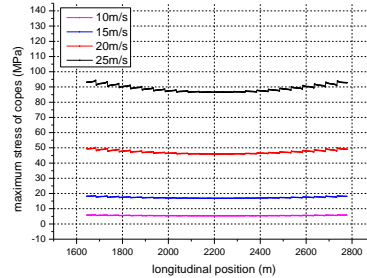


Fig. 17 wind-induced tensile stress of rope with varying wind velocity (+3° attack angle)

Usually typical catwalk will present aerodynamic divergence at high wind speed with small torsional deformation, say 8° (Zheng 2007). However, for this integrated type, it can clearly say that aerodynamic divergence will not occur at wind speed of 25 m/s even though the maximum torsional deformation is up to 23°, since the displacements show no sign of dramatic change. Such behaviour is totally unpredicted based on the understanding of the typical type. Therefore, the author tried to solve the query from the following two aspects:

1. The stiffness of cable elements is larger at higher wind speed. The cable element stiffness is generated from axial stresses, which are produced by gravity and wind load. The gravity part is constant, but the wind-induced part varies. Higher wind speed will induce much larger additional stiffness to the cable elements. Fig. 17 shows the floor rope axial stress along the catwalk under different wind speeds. It is noted that the gravity induced tensile stress of cable ranges from 256 MPa to 315 MPa, and the frequency of first antisymmetric torsional mode increases from 0.104 Hz to 0.116 Hz as wind speed reaches 25 m/s.

2. The integrated catwalk is more flexible without large connecting bridges acting as strong restraints, so it can deform more easily to form a more compactible shape under higher loading, while the typical catwalk is more likely to perform sudden deformation change at position with existence of a certain connecting bridge.

3.5 Measure to reduce the deformation

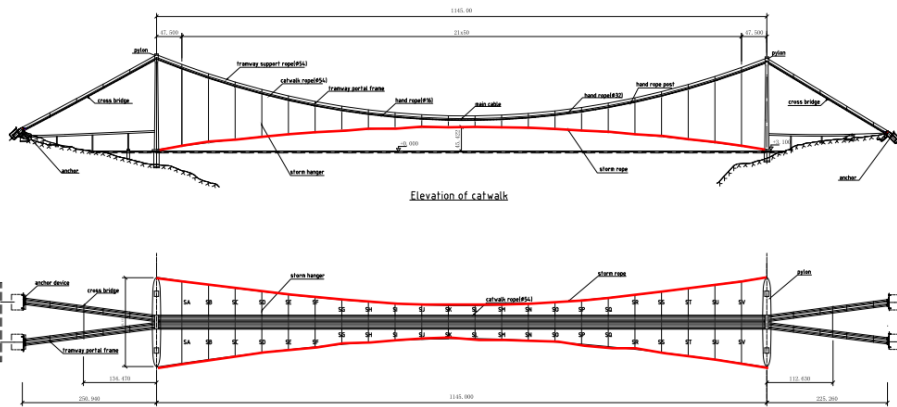
The integrated catwalk has smaller stiffness than the typical type, and produces large displacements under strong wind, which have been verified by the above numerical analysis. Although aerodynamic divergence does not occur at the design wind speed, the torsional deformation is so large that it could cause unsafety issues for construction. For example, if unexpected gust occurs, it could produce large deformation in a short time, which could make the workers fall down and get injured.

Similar to the typical catwalk (Ito *et al.* 1976), the most effective measure to reduce the displacement is the storm rope system. Model with storm rope system was also developed in ANSYS. Storm rope system arrangement and the ANSYS model are shown in Fig. 18.

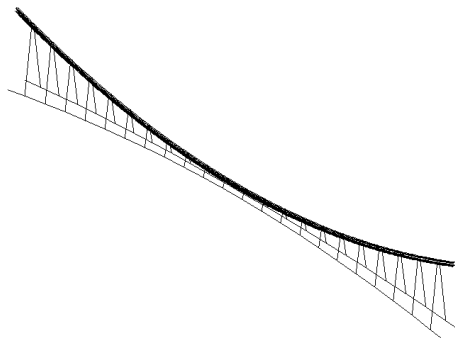
The storm rope system consists of two ropes that are connected with the catwalk supporting ropes by hanger ropes. The diameter of the storm ropes is same as the catwalk supporting ropes. Obviously, the storm rope system can effectively enhance the catwalk stiffness especially for the lateral and torsional, and thus reduce the deformation to acceptable level.

Deformation comparison for models with and without storm rope system was shown in Fig. 19. The lateral and torsional deformation reduced half and the vertical deformation was only a quarter of that without using storm rope system.

It must be pointed that special attention should be paid to design of storm ropes, because deformation reduction ratio of the catwalk is very sensitive to the initial tension of storm ropes. The initial tension of the storm ropes should not be too high, not only to effectively control the catwalk deformation but also avoid causing anchorage problem to pylons.



(a) Storm rope system in plan view and elevation view



(b) finite element model catwalk with storm cable

Fig. 18 Storm rope of catwalk

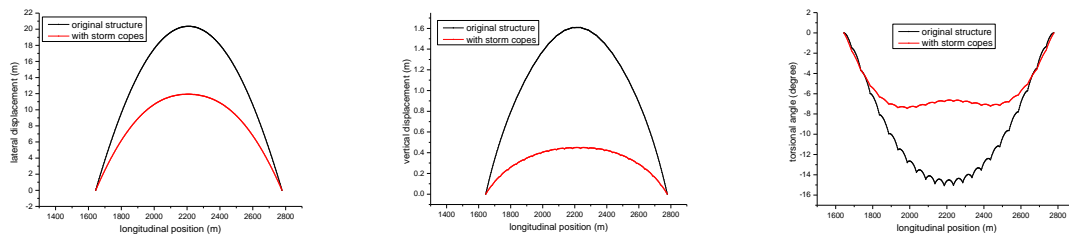


Fig. 19 Comparison on catwalk deformation with or without storm cable (20 m/s, zero initial wind angle of attack)

4. Conclusions

To investigate aerodynamic responses for integrated catwalk structure, wind tunnel tests and nonlinear numerical analysis were conducted in this paper. The main findings are summarized in the following: According to wind tunnel tests, it is noted that the drag coefficients of the integrated catwalks are much larger than the typical type. The drag coefficients are strongly affected by vertical mesh solidity ratio. The lift and pitching moment coefficients are more related to number of vertical meshes installed rather than the solidity ratio of the vertical member. Simple fitting formulas were proposed to estimate the aerodynamic coefficients of the integrated catwalk under specified solidity ratio.

In theory, it revealed that lateral deformation of integrated catwalk could significantly affect the vertical and torsional motion, and it contributes the majority of the torsional deformation. This was verified by numerical analysis as well.

From numerical analysis and comparing with study on typical catwalk, it is found that the deformation of the integrated catwalk is much larger due to the smaller stiffness. However, it does not show aerodynamic divergence even though torsional deformation is up to 20°. Considering safety for construction, storm rope system is proposed to reduce the deformation to acceptable level.

Acknowledgments

This research was supported by the granted projects (NO. U1434205, NO. 51308478 and NO. 51678508) from the China Natural Science Funding, and was also supported by the granted project (NO. KLWRTBMC13-04) from the Key Lab for Wind Resistance Technology of Bridges of the Transport Ministry. The technique documents provided by the Sichuan Road and Bridge Group co. LTD.

References

- Akiyama, M., et al. (1999), "Erecting technology for suspension bridge cables", *Bridge Constr. Eng.*, **49**(2), 2-7 (in Japanese).
- Allan Larsen (1993), "Aerodynamic aspects of the final design of the 1624 m suspension bridge across the Great Belt", *J. Wind Eng. Ind. Aerod.*, **48**, 261-285.
- Allan Larsen. (1997), "Prediction of aeroelastic stability of suspension bridges during erection", *J. Wind Eng. Ind. Aerod.*, **72**, 265-274.
- Cheng, J., Jiang, J.J., Xiao, R.C. and Xiang, H.F. (2002), "Nonlinear aerostatic stability analysis of Jiangyin suspension bridge", *Eng. Struct.*, **24**(6), 773-781.
- Gimsing, N.J. (2012), *Cable supported bridges: Concept and design*, Wiley, Chichester, U.K.
- Honshi Technical Rep. (1974), "Honshu- Shikoku Bridge Authority", Kobe, Japan (in Japanese).
- Kawaguchi, K. and Fukunaga, S. (1995), *Structure of catwalk on the Akashi Kaikyo Bridge*.
- Kwon, S.D., Lee, H., Lee, S. and Kim, J. (2012), "Dynamic wind actions on catwalk structures", *Proceedings of the 7th International Colloquium on Bluff Body Aerodynamics and Applications (BBAA7) Shanghai, China*, September 2-6.
- Kwon, S.D., Lee, H., Lee, S. and Kim, J. (2012), "Mitigating the effect of wind on suspension bridge catwalks", *J. Bridge Eng.*, **18**(7), 624-632.
- Li, S. and Ou, J. (2009), "Analysis of dynamic behavior of catwalks of long-span suspension bridge without

- wind-resistant cable”, *J. Highway Transportation Research Development*, **26**, 47-53.
- Li, S., Hu, Y., Du, D., et al. (2015), “Numerical analysis of aerostatic coefficients of catwalks of long-span Suspension Bridge”, *J. Zhengzhou University (Engineering Science)*, **34**(4), 57-61, (in Chinese).
- Li, Y., Wang, D., Wu, C., Chen, X. et al. (2014). “Aerostatic and buffeting response characteristics of catwalk in a long-span suspension bridge”, *Wind Struct.*, **19**(6), 665-686.
- Ito, M., Miyata, T. and Sugita, Z. et al. (1976), “Study on wind-resistant performance of catwalk structures”, *Proceeding of the 4th Symposium on wind engineering in Japan*, December, Tokyo. (in Japanese).
- Shinichi, H., et al. (1997), “Design and construction of the catwalks for the Kurushima Bridges”, *Bridge Found. Eng.*, **31**(6), 13-19, (in Japanese).
- Tanaka, H. (1998). “Aeroelastic stability of suspension bridges during erection”, *Struct. Eng. Int.*, **8**(2), 118-123.
- Thai, H.T. and Kim, S.E. (2011), “Nonlinear static and dynamic analysis of cable structures”, *Finite Elem. Anal. Des.*, **47**(3), 237-246.
- Uejima, H., Inoue, M., Yamauchi, K., et al. (2014), “Izmit bay suspension bridge-aerodynamic stability of catwalk”, IABSE Symposium Report. International Association for Bridge and Structural Engineering, 2041-2048.
- Wang, J., Li, Y., Liu J., et al. (2013), “Nonlinear aerostatic response of catwalk of suspension bridge”, *J. Highway and Transportation Research Development*, **7**(2), 40-45
- Wang, Z, Luo, Z. and Guo, J. (2015), “Design and study of wind-resistant stability to the catwalk of the Guanshan bridge”, *Highway*, **1**, 67-71, (in Chinese).
- Zheng, S., Liao, H. and Li, Y. (2007), “Stability of suspension bridge catwalks under a wind load”, *Wind Struct.*, **10**(4), 367-382.
- Zheng, S.X. and Liao, H.L. (2002), “Study on the stability of catwalk of suspension bridges”, *Proceeding of the 2nd International Symposium on Advances in Wind & Structures*, 21-23, August, Busan, Korea.